JGR Earth Surface

RESEARCH ARTICLE
10.1029/2019JF005493

Detailed Bathymetry of the Continental Shelf Beneath the Getz Ice Shelf, West Antarctica

James R. Cochran[1], Kirsty J. Tinto[1], and Robin E. Bell[1]

[1]Lamont-Doherty Earth Observatory, Columbia University, Palisades, NY, USA

Key Points:
- Inversion of airborne gravity data for bathymetry shows the Getz Ice Shelf to consist of three separate cavities with only shallow (<400 mbsl) connections between them
- Within each cavity, deep troughs extend from the ice front to the grounding line, allowing warm modified Circumpolar Deep Water access to the inner ice shelf

Supporting Information:
- Supporting Information S1

Correspondence to:
J. R. Cochran,
jrc@ldeo.columbia.edu

Citation:
Cochran, J. R., Tinto, K. J., & Bell, R. E. (2020). Detailed bathymetry of the continental shelf beneath the Getz Ice Shelf, West Antarctica. *Journal of Geophysical Research: Earth Surface*, *125*, e2019JF005493. https://doi.org/10.1029/2019JF005493

Received 17 DEC 2019
Accepted 11 SEP 2020
Accepted article online 25 SEP 2020

Abstract The Getz Ice Shelf (GIS) produces major amounts of basal meltwater due to intrusions of warm modified Circumpolar Deep Water (mCDW) beneath the ice shelf. However, multiple cavity openings and complex geography mean that knowledge of bathymetry beneath the GIS is required to understand ice/ocean interactions. We invert NASA airborne gravity data to obtain bathymetry beneath the ice shelf. Our gravity/geology-constrained bathymetry is a significant advance on Bedmap2 bathymetry. The sub-ice shelf bathymetry consists of three cavities separated by topographic ridges extending from the ice shelf front to the grounding line. Passages allowing limited circulation of shallow ($\lesssim$400 meters below sea level [mbsl]) water between cavities are present, but deeper water is confined to individual cavities. Within each cavity, bathymetric troughs (>900 mbsl) extend from the ice shelf front to subglacial valleys beneath the ice sheet. Our analysis of the gravity data also allows us to infer the presence of thick (>500 m) sediments near the grounding line through much of the GIS, as well as variations in the density and/or thickness of the crust underlying the ice shelf.

Plain Language Summary Floating ice shelves surrounding Antarctica slow the flow of the Antarctic Ice Sheet toward the ocean. West Antarctic ice shelves, including the large Getz Ice Shelf, have thinned significantly over the past 20 years, due in part to increased flow of warming ocean water into the ocean cavities beneath them. This thinning results in acceleration of ice flowing into the ocean, so that more ice goes afloat, raising sea level. We mapped the shape of the ocean floor beneath the Getz Ice Shelf, which controls water circulation under the ice shelf. We found the ice shelf has three separate portions each with deep troughs that provide pathways for warm water to the edge of the ice sheet.

1. Introduction

Floating ice shelves are a widespread feature of the Antarctic coastal region, bordering as much as 75% of the coast (Rignot et al., 2013), and are also an important control on Antarctic mass balance. Since they are already floating, thinning or disintegration of ice shelves does not directly affect sea level. However, ice shelves serve to stabilize and buttress adjacent grounded ice sheets, so their removal enhances flow of grounded ice into the ocean, accelerating sea level rise (e.g., Dupont & Alley, 2005; Gudmundsson, 2013).

Ice shelves around Antarctica show a net mass loss extending over the past two decades (e.g., Paolo et al., 2015; Rignot et al., 2013). Ice shelf mass loss occurs through both calving and basal melting (Jacobs et al., 1992), with many recent studies emphasizing the role of basal melting (e.g., Depoorter et al., 2013b; Liu et al., 2015; Pritchard et al., 2012; Rignot et al., 2013). Ice shelves facing the Amundsen and Bellingshausen seas are particularly susceptible to basal melting due to intrusions of warm Circumpolar Deep Water (CDW) or its cooler modified derivatives (mCDW) onto the West Antarctic continental shelves (e.g., Assmann et al., 2019; Jacobs et al., 1996, 2012; Thoma et al., 2008). The rapid thinning and grounding line retreat experienced by the large glaciers feeding into the eastern Amundsen Sea Embayment (ASE) has been widely attributed to penetration of CDW into their shelf cavities (e.g., Jacobs et al., 2011; Jenkins et al., 2010; Rignot, 2008; Seroussi et al., 2017; Shepherd et al., 2004; Turner et al., 2017).

The Getz Ice Shelf (GIS), with a surface area of ~34,000 km^2, extends for ~650 km along the central and western portion of the Amundsen Sea coast of West Antarctica with a width that varies from ~40 to >100 km (Figure 1). Two significant glaciers, Berry Glacier and DeVicq Glacier, feed into the western portion of the GIS (Figure 1) and occupy deep, narrow subglacial valleys evident in onshore radar data. The ice shelf is bounded on its seaward side by a series of islands that pin it and define its seaward boundary. Three of the islands contain outcropping volcanoes that were active in the Pleistocene (Shepard and Grant islands)

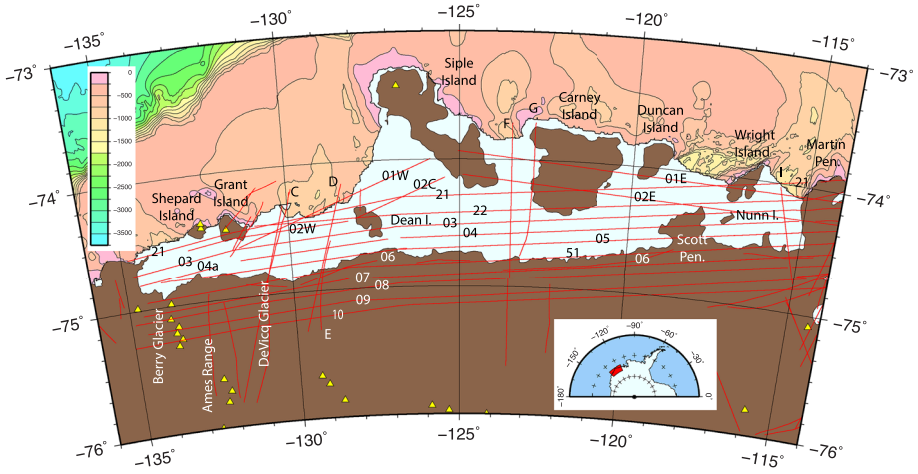

Figure 1. Map of the Getz Ice Shelf with location of Operation IceBridge gravity lines shown in red. Lines are labeled as referred to in the text. Islands and other geographic features discussed in the text are also labeled. Yellow triangles show the location of outcropping Neogene volcanics. Bathymetry seaward of the ice shelf is from International Bathymetric Chart of the Southern Ocean (IBCSO) (Arndt et al., 2013). Color scale for the bathymetry in meters is shown in the inset on the upper left. Inset on the lower right shows the location of the map on the West Antarctic coast.

or Quaternary (Siple Island) (LeMasurier, 1990). These volcanic terrains suggest lateral variations in the nature of the crustal rocks beneath the ice shelf.

Jacobs et al. (2013) analyzed an extensive set of conductivity-temperature-depth (CTD) and dissolved oxygen profiles from oceanographic stations along the GIS cavity openings and further north on the continental shelf. They found significant west-to-east variations along the ice front in surface water structure and in depth to the thermocline, as well as marked interannual variations. However, despite these variations, water below a depth of about 500 m was found to be consistently at least 1–2° above the in situ freezing point. Jacobs et al. (2013) also utilized their data to calculate seawater transport into and from the cavity along with melt water transport and to estimate basal melting of the ice shelf. They found that the amount of basal melt varied significantly with average rates of 1.1 m/yr in the year 2000 (deeper thermocline) and 4.1 m/yr in 2007 (shallower thermocline). The latter estimate fell within the time period of a 4.3 ± 0.4-m/yr determination of ice melting by Rignot et al. (2013) for the period 2003–2008 from satellite measurements and a surface mass balance model. Paolo et al. (2015) determined a mean thinning rate of 16.1 ± 1.5 m/decade (1.6 m/yr) over the period 1994–2012 for the GIS from satellite altimeter measurements and isostasy.

Assmann et al. (2019) found a persistent year-round flow of warm water toward the Getz cavity at two moorings located ~15 km seaward of the ice front just west of Siple Island. However, the complex nature of the GIS, with numerous cavity openings, unknown bathymetry beneath the ice shelf, and uncertain connectivity for water flow behind the islands, lends uncertainty to models of circulation within the cavity. Knowledge of the bathymetry beneath the ice shelf is necessary to determine the geometry of the seawater cavity and to assess sub-ice shelf circulation and its effect on basal melting.

The most widely used grid for bathymetry beneath the GIS is from Bedmap2 (Fretwell et al., 2013) (Figure 2). This bathymetric model utilized a spline technique to interpolate between the Nitsche et al. (2007) grid of shipboard bathymetric data seaward of the ice shelf and Bedmap2 bed elevation data under the ice sheet and islands (le Brocq et al., 2010; Timmermann et al., 2010). The Bedmap2 ice keel grid was used to adjust ("excavate") the seafloor when the interpolation produced grounded ice at locations where it is known to be floating (le Brocq et al., 2010). No other geological or geophysical information from the region of the ice shelf was utilized. le Brocq et al. (2010) state "no claims are made about the accuracy of the sub ice-shelf interpolation, only that it is a 'best guess' and it allows the ice shelf to float."

The Bedmap2 sub-ice bathymetry shows a rather featureless seafloor marked by a steady deepening away from the ice sheet and islands toward the seaward edge of the ice shelf (Figure 2). This pattern is in contrast to the bathymetry observed by shipboard swath mapping just seaward of the GIS, where distinctive deep

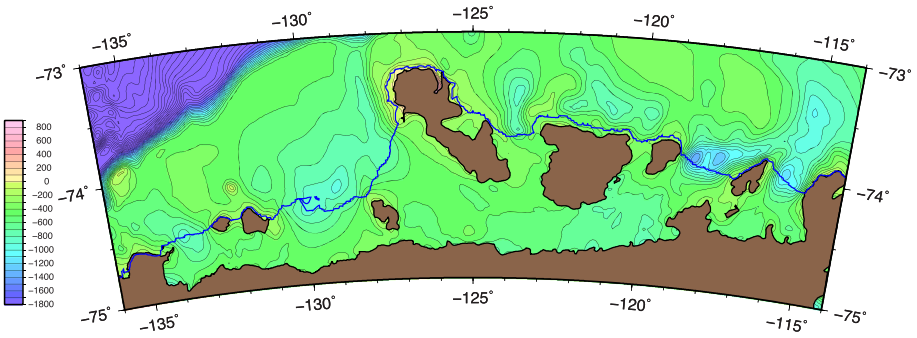

Figure 2. Bedmap2 bathymetry beneath the Getz Ice Shelf and adjacent continental shelf (Fretwell et al., 2013) gridded with 2-km node spacing and contoured at 100-m intervals. Color scale for the bathymetry in meters is shown in the inset on the left and is identical to the color palette used for our new bathymetry in Figure 9. Heavy blue line shows the approximate seaward edge of the ice shelf. The sub-ice shelf Bedmap2 bathymetry is an interpolation between ice penetrating radar-determined sub-ice topography in Marie Byrd Land and ship-determined bathymetry from International Bathymetric Chart of the Southern Ocean (IBCSO) (Arndt et al., 2013) seaward of the ice shelf.

troughs and shallower banks are observed (Figures 1 and 2). A better model for bathymetry beneath the GIS is clearly necessary to consider possible effects of warm subthermocline water on the evolution of the ice shelf.

Inversion of airborne gravity data is an extremely efficient method to determine bathymetry beneath an ice shelf as extensive as the GIS (e.g., Cochran et al., 2014; Cochran & Bell, 2012). NASA's Operation IceBridge (OIB) has systematically collected airborne geophysical data over West Antarctic ice shelves including the GIS (Figure 1). Here, we invert OIB airborne gravity data to obtain a geologically consistent estimate of the bathymetry beneath the GIS. The gravity inversion included in the recently published Bedmachine Antarctica topography/bathymetry model (Morlighem et al., 2020) did not explicitly address effects of sediments and lateral changes in crustal structure on the resulting bathymetry (Millan et al., 2020), both of which we find in this study to have significant effects on results of the inversion.

2. Inversion of Gravity Data for Bathymetry Beneath the GIS

OIB obtained low-altitude (~500 m) airborne geophysical data over the GIS on eight flights during six different campaigns between 2009 and 2016 (Figure 1). These flights collected data along a series of long east-west lines spaced at 10- to 15-km intervals from near the ice front to ~50 km landward of the grounding line. These lines were crossed at irregular intervals by north-south geophysical lines, several of which extended from landward of the grounding line across the full width of the ice shelf to the continental shelf seaward of the GIS. Flights were flown at a nominal height of 1,500 ft (457 m) above the Earth's surface. Instrumentation on these flights included a laser altimeter, a variety of ice-penetrating radars, and a gravimeter.

Ice thickness was measured using the Multichannel Coherent Radar Depth Sounder (MCoRDS) developed and operated by the University of Kansas Center for Remote Sensing of Ice Sheets (CRESIS) (Allen et al., 2010; Leuschen, 2011). Gogineni et al. (2014) report mean thickness mismatches of ~35 and ~30.6 m with standard deviations of ~40.7 and ~40.0 m for detailed surveys in Greenland and Antarctica. On OIB lines over the GIS, ice thickness mismatches at crossovers ranged from 0.2 to 85.0 m with a standard error of 19.7 m.

Surface elevation along the profiles was determined with the NASA Airborne Topographic Mapper (ATM) laser altimeter (Krabill, 2014). OIB surface elevation data are referenced to the WGS-84 ellipsoid, so we corrected the data to sea level using the GL04C geoid (Förste et al., 2008). This geoid was also used as a datum for Bedmap2 (Fretwell et al., 2013). The accuracy of elevations recovered from the ATM system has been estimated at about 10 cm (Krabill et al., 2002; Martin et al., 2012). For the ATM lines over the GIS, the mismatches at crossovers ranged from 0.0 to 16.8 m with a standard error of 3.7 m. Part of the mismatch, for both ATM and radar crossovers, is due to the fact that the data were collected over a 7-year period. The

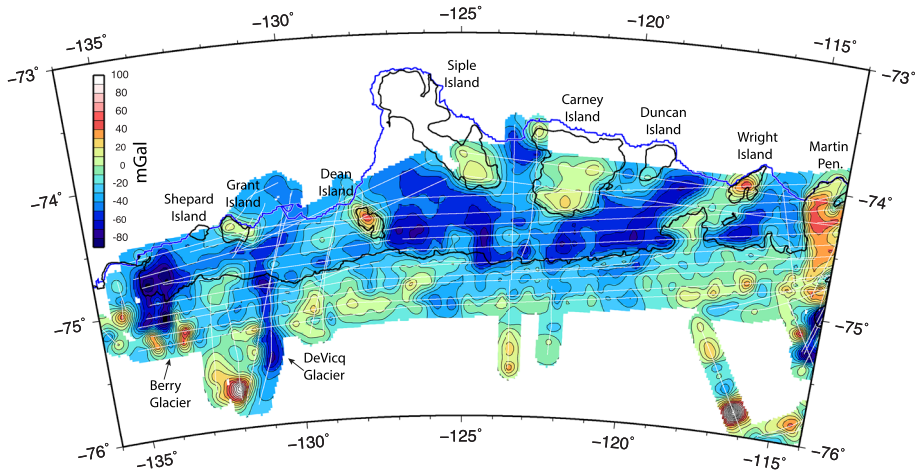

Figure 3. Free-air gravity anomalies from OIB flights over Getz Ice Shelf and adjacent areas gridded with 2-km node spacing and contoured at 10-mGal intervals. Inset in upper left shows color scale for gravity anomalies. Data l ocations are shown in white. Areas >10 km from a data point are masked. Thick black lines show the Depoorter et al. (2013a) grounding line along the ice sheet and the 75-m elevation contour on the islands. Heavy blue line shows the approximate seaward edge of the ice shelf.

GIS is a dynamic system, and both surface elevation and ice thickness at any location are not constant over that time. Tidal displacements also contribute ~0.5- to 1.0-m elevation uncertainty (e.g., McMillan et al., 2011; Padman et al., 2002). In addition, we used data sampled at 200-m intervals along-track for our study. We here compare the sampled results, so there is a degree of interpolation involved in determining the crossover mismatch.

ATM data were not available for Line 03 and for portions of Lines 04 and 21. For those, we used surface elevation data from CRESIS radar. Crossovers of those line segments with north-south lines gave nearly identical statistics to the ATM data, with a mismatch range of 0.2–12.1 m and standard error of 3.7 m.

2.1. Gravity Anomalies Over the GIS

Gravity measurements on OIB flights (Tinto et al., 2019) were made with a Sander Geophysics Ltd. Airborne Inertially Referenced Gravimeter (AIRGrav) system (Argyle et al., 2000; Sander et al., 2004). An advantage of the AIRGrav system is that it is able to collect high-quality data during draped flights (Studinger et al., 2008) such as those undertaken on OIB deployments. The free-air gravity anomalies were filtered with a 70-s full-wavelength filter, resulting in an along-track half-wavelength resolution of ~4.5 km for a typical flying speed of 250 knots (128.6 m/s). This implies that the full amplitude of features wider than ~5 km will be resolved in the gravity data.

Free-air gravity anomaly mismatches at line crossings range from 0.0 to 5.0 mGal with a standard error of 1.29 mGal. Many of the larger crossover discrepancies appear to be the result of the along-track filtering applied to the gravity data during processing, which means that the value at a particular point is affected by measurements for half of the filter width in each direction along the track. This along-track filtering can lead to mismatches at the intersection of orthogonal lines where the along-track variations in gravity may be very different in the two directions. This is illustrated by the observation that three of the five largest crossover mismatches are at the intersection of Line G with Lines 01E, 02E, and 21 along the western margin of Carney Island (Figure 1). All three of the east-west lines have significant along-track gravity gradients at the intersection location, while the north-south Line G was flown approximately along the gravity contours (Figure 3).

A map of the free-air gravity anomalies over the GIS, gridded with 2-km node spacing and contoured at 10-mGal intervals is shown in Figure 3. The general level of the free-air gravity anomalies is negative throughout most of the ice shelf. Gravity highs are found over the islands, often reaching positive values. Maximum observed free-air anomalies are on the order of 50 mGal over the Martin Peninsula, Wright Island, and Dean Island. Areas of negative anomalies are found between the islands, taking the form of

troughs extending from the ice front toward the grounding line. Two of the largest amplitude gravity troughs are associated with DeVicq Glacier at about 131°W and Berry Glacier at 134°W. The gravity trough associated with DeVicq Glacier extends from east of Grant Island to at least 80 km up onto the ice sheet. OIB radar shows it to overlie a narrow valley beneath the grounded ice sheet that reaches 1,570 m above sea level (mbsl) at 75°29.6′S with a minimum recorded gravity anomaly of −73.6 mGal. Minimum gravity anomalies over the ice shelf seaward of this trough are in the range of −45 to −60 mGal. The gravity low over Berry Glacier does not extend as far landward, but reaches a minimum of −104 mGal on Line 07, ~10 km landward of the grounding line, where radar shows a bed depth of 1,949 mbsl. Gravity anomalies over the ice shelf seaward of Berry Glacier show a broad area with anomalies reaching −80 to −95 mGal. Other gravity troughs, reaching −70 to −75 mGal, extend between Siple and Dean islands and between Wright and Duncan islands. The gravity trough between Martin Peninsula and Wright Island has minimum values of −50 to −60 mGal. Ridges of relatively high gravity extend from Wright Island to the Scott Peninsula and from Dean Island to the mainland. Other less continuous areas of relatively high gravity are found west of Dean Island and southwest of Carney Island.

2.2. Inversion of Free-Air Anomalies for Bathymetry

Inversion of the gravity data for bathymetry utilized the Geosoft GMSys profile modeling software package. This software does iterative forward modeling using the method of Talwani et al. (1959) to model the bathymetry and calculate the gravity anomaly resulting from the inversion. The base of floating ice and the bed in grounded areas were both kept fixed at the depths observed with radar, and the bathymetry in water-covered areas varied to minimize the RMS difference between the observed gravity profile and the free-air gravity calculated from the model. Densities of 2.67 g/cm^3 for rock, 0.915 g/cm^3 for ice, and 1.03 g/cm^3 for seawater were used in the modeling.

An important step in the inversion process is the appropriate choice of the density reference column for each profile. This process, commonly referred to as "pinning" the gravity, defines a location on the profile where the depth to the inverted for surface is held constant, which is used to determine the offset between the observed and calculated gravity data. The density structure at the pinning location, which depends on the local density and thickness of the crust and sediment, is assumed for the entire length of the profile being inverted. The inversion will interpret any gravity anomaly due to subsurface density variations (e.g., a thinning or thickening of sediments) as resulting from relief on the surface that it is determining, in our case the seafloor. It is thus essential that the "pinning point" density structure is characteristic of the region over which the seafloor depth is required (Boghosian et al., 2015). Pinning points used for each line are given in Table S1.

2.2.1. "Pinning" the North-South Lines: Presence, Location, and Approximate Thickness of Sediments

For lines that extend seaward of the ice shelf to areas where the seafloor has been mapped by shipboard swath mapping, we established density reference columns just seaward of the ice shelf within the region of mapped seafloor, holding the depth there at the depth obtained from the International Bathymetric Chart of the Southern Ocean (IBCSO) bathymetric grid (Arndt et al., 2013). For each profile, we took care that our reference column was from a location with depths well determined by swath data in regions of exposed bedrock with little or no sediment cover.

This choice of where to pin the inversions was based on shipboard seismic studies of sediment distribution on the continental shelf. Wellner et al. (2001) and Lowe and Anderson (2002, 2003) used seismic reflection data to establish a pattern of thick sediments characterized by seaward dipping reflectors on the outer continental shelf and exposed bedrock with minimal amounts of sediment on the inner shelf of the eastern ASE seaward of Pine Island Bay. Larter et al. (2009) and Graham et al. (2009) used seismic data to show that this pattern extends westward to the north of the GIS at least to Carney Island and that the contact between exposed bedrock and the sedimented outer shelf is at about 73°30′S. Seismic reflection profiles north of the western half of the GIS have not been published. However, Wellner et al. (2001) report geomorphic bedforms characteristic of bare rock on the inner portion of the continental shelf in Wrigley Gulf (area west of Siple Island), changing to features typical of sedimented regions on the outer shelf. It thus appears that our density reference columns tied to the mapped seafloor just seaward of the ice shelf are on bedrock covered with no or minimal sediments.

Based on observations in the eastern Amundsen Sea, seaward of Pine Island Bay (Lowe & Anderson, 2002, 2003), we assume that this region of minimal sediment extends under the ice shelf to near the grounding line. However, close to the eastern ASE grounding line, Nitsche et al. (2013) found a zone just seaward of the Pine Island ice shelf with up to 300 m of sediment filling topographic depressions, and Muto et al. (2013, 2016) utilized a nonlinear statistical technique to infer a basin with 800 m of sediment near the current Pine Island Glacier grounding line. These observations raise the possibility that thick sediment accumulations may also exist in overdeepenings near the GIS grounding line.

Our inversions do suggest thick sediment accumulations near the grounding line, at least in the central and western portion of the GIS. In addition to the inversions with density reference columns tied to acoustically determined shipboard bathymetry, we did inversions of the N-S lines with density reference columns located on the radar-defined bed just landward of the grounding line. Results for Line C, located east of Grant Island in the western GIS, and Line I, between Wright Island and the Martin Peninsula in the easternmost GIS, are shown in Figure 4. For both lines, the seafloor determined from an inversion with a density reference section established on mapped seafloor is shown by a solid red line and underlying brown region. The calculated gravity anomaly is also in red. The bathymetry and gravity anomalies calculated from an inversion pinned just landward of the grounding line are shown as broken black lines. In grounded areas, the bed is the same for both inversions since it was not allowed to vary but was held at the elevation observed on radar data.

Bathymetry determined by the inversion for Line C pinned just landward of the grounding line is immediately below the base of the ice (and would be shallower if allowed) from the grounding line to the seaward edge of a grounded area and ice rise located from −30.4 to −27.4 km on our profile. Seaward of the ice rise, bathymetry from this inversion parallels the bathymetry from the inversion pinned to mapped seafloor, but is ~400 m shallower. This shallow seafloor is the result expected if the bed beneath the density reference column just landward of the grounding line includes a significant thickness of sediment that is not present seaward of the ice rise. As the sediment thickness decreases across the seaward boundary of the local basin, the inversion process will interpret shallowing of the buried sediment/bedrock interface as shallowing of the water/seafloor interface, resulting in depths that are too shallow.

Assuming an average sediment density of 2.2 g/cm^3, the calculated bathymetry will be too shallow by about 30 m for every 100-m decrease in sediment thickness (Cochran et al., 2014). Thus, assuming this average sediment density, the ~400 m offset between the two bathymetry profiles implies the presence of ~1,300 m of sediment at the pinning point. The sediments must thin rapidly seaward of the grounding line, since the grounded ice under the ice rise appears to be sitting on bedrock. The conclusion that the ice rise is bedrock results from the observation that bathymetry produced by pinning the gravity at the ice rise is within ~30 m of that produced by pinning on open seafloor.

Turning the calculations around, the large overdeepening between the grounding line and ice rise on the inversion of Line C tied to open seafloor (Figure 4) arises from the landward decrease in gravity resulting from the subsurface change from bedrock to sediment being interpreted as relief on the seafloor and is not real. Since we do not know the basement configuration between the ice rise and the grounding line, we cannot confidently model the seafloor in that region other than to say it must be much shallower than in our inversion.

For Line I, at the far eastern end of the GIS, inversions pinned to the seafloor and to the bed just landward of the grounding line gave very similar bathymetric profiles with a mean difference of 24.7 $\pm$ 16.2 m, indicating that there is not a thick deposit of sediments near the grounding line at this location.

Similar analyses imply sediment accumulations at all of our N-S profiles other than Profile I. Comparison of inversions pinned on open seafloor and at 1–2 km landward of the grounding line yield sediment thickness estimates at the landward pinning point of ~400 m for Line D and ~800 m for Line F.

Line E does not extend to the open ocean. We inverted Line E by pinning it at its crossing with Line 04 to an inversion of Line 04 that was pinned to our Line D inversion. Comparison of this inversion with one pinned landward of the grounding line suggests ~900 m of sediment near the Line E grounding line.

The landward limit of the gravity data on Line G is just seaward of the ice sheet grounding line, preventing us from carrying out an inversion pinned landward of the grounding line. Gravity data on Line G also do not reach to open ocean north of Carney Island (Figure 1). We did two inversions of Line G, one with a

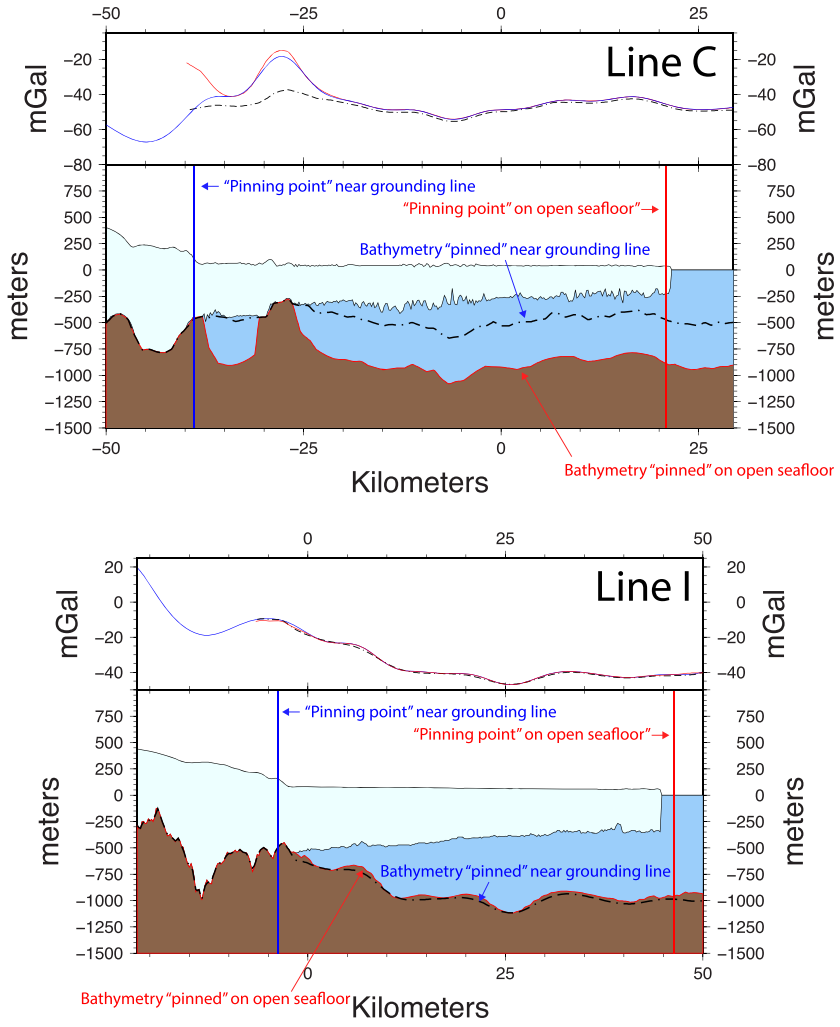

Figure 4. Comparison of results obtained for Line C (top) and Line I (bottom) with two different density reference columns. For each line, the bathymetry obtained with a density reference column on mapped seafloor just seaward of the ice shelf is shown in red and is underlain by the solid brown area. The bathymetry obtained with a density reference column on radar-determined bed just landward of the grounding line is shown as a broken black line. The upper panel for each profile shows the observed free-air gravity in blue, the gravity anomaly predicted with a density reference column on open seafloor in red and the gravity anomaly predicted with a density reference column near the grounding line as a broken black line. For Line C, the "open seafloor" reference column is now under the ice shelf due to an advance of the ice front between the times of the shipboard measurements and the OIB flight.

density reference column on Carney Island and the other pinned to the intersection with an inversion of Line 04, which is in turn pinned to Line F. The two are nearly identical with a mean difference of 23.0 ± 24.2 m over floating ice. Both inversions of Line G both show a large overdeepening reaching 1,365 mbsl about 5 km seaward of the grounding line. By analogy with the other N-S lines, including in particular Line F, ~10 km to the west (Figure 1), we conclude that thick sediments are present near the Line G grounding line.

There are factors other than sediments that can affect the inversion including, in particular, intrusions into the crust. However, to produce the observed effects on the inversion, any intrusion would need to be aligned in a relatively narrow band, 10–20 km wide and several hundred km long, parallel to and straddling the grounding line. Such an alignment would be very fortuitous. An observation strongly suggesting that sediments are the low-density material affecting the inversions is that the low-density material is constrained to occupy an overdeepening located immediately landward of an ice rise where the ice is grounded on bedrock on Line C (Figure 4).

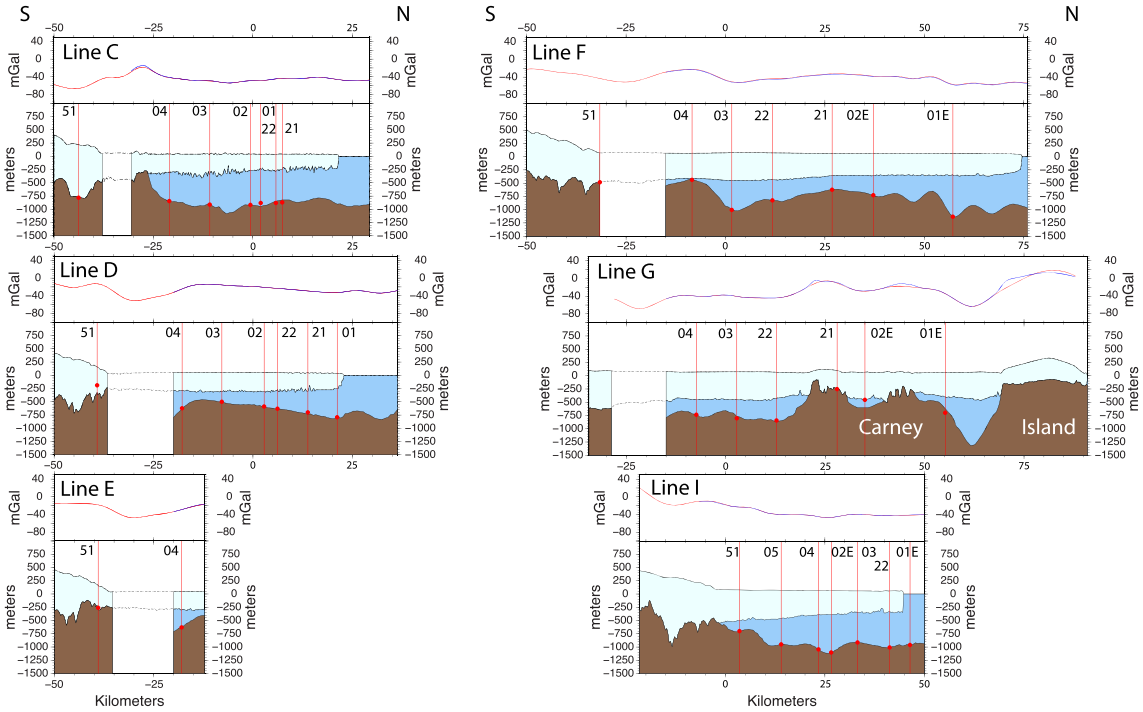

Figure 5. North-south geophysical profiles across the Getz Ice Shelf (locations shown in Figure 1). For each line, the upper panel shows the observed free-air gravity in red and the anomaly predicted by the inversion in blue. Lower panels show OIB geophysical profiles. Upper and lower surfaces of the ice are from lidar and radar, respectively. Where ice is grounded, the bed is determined from radar measurements. Where ice is floating, bathymetry is from inversion of gravity anomalies. Gaps in the bed just seaward of the grounding zones show areas where we deduce the presence of thick sediments. Vertical red lines show intersections with east-west lines. Bathymetry/bed depth on the cross lines is shown as red dots. All lines are projected along N0°E. The distance origin for each profile is at 74°30′S.

We can constrain the seaward extent of the thick sediments on Line C, since they must be landward of the ice rise crossed on that profile, where the ice is grounded on bedrock. On the other lines, we can estimate the sediment thickness at a pinning point 1–2 km landward of the grounding line but cannot constrain how far seaward the sedimentary basin extends and thus how far seaward of the grounding lines our inversions tied to nearly sediment-free seafloor are in error. All of the profiles (other than Line I) show an overdeepening seaward of the grounding line, which appears to be, at least in part, an artifact due to the presence of sediments that our inversions, pinned seaward of the ice shelf, interpreted as relief on the bed. We have chosen to cut off our inversions where there is an inflection point toward rapidly deepening seafloor going in a landward direction. Our final N-S profiles, with the portions in which we do not trust the inversions removed, are shown in Figure 5.

2.2.2. "Pinning" the East-West Lines: Variations in Crustal Structure

Inversions of the east-west lines, whether pinned to mapped seafloor (possible for Lines 21, 01E, and 01 W) or to any of the N-S lines, all imply grounded ice along two ridges extending from near the ice front to the grounded ice sheet. Radar data on all of the east-west lines also indicate grounded ice at these locations. These ridges comprise Wright Island and the Scott Peninsula near 117°30′W, and Dean Island near 127° 30′W (Figure 1). We will consider these ridges in more detail below.

This observation allows us both to improve the resolution of the inversion results and to identify and correct for variations in crustal structure along the ice shelf. Since the inversion software has a maximum number of nodes, dividing the E-W profiles into segments broken at these zones of grounded ice allows us to increase the resolution of the results. In addition, comparison of inversions tied to different N-S profiles also allows us to explore the possibility of changes in crustal structure along the length of the GIS. Given that the ice shelf extends for ~650 km, variations in bedrock geology are likely.

Line I, which extends beyond the ice shelf to mapped seafloor where water depths are known from shipboard swath mapping, was used as a master line for the region to the east of the Wright Island Ridge. It

was inverted with a density reference column established at its crossing with Line 01E, which occurs within the mapped seafloor. The same location was used as the pinning point for Line 01E. Each of the other eastern east-west lines was pinned to Line I by establishing a density reference column at the intersection with Line I with the depth at that location held at the depth on the Line I inversion. The one exception was Line 21, which passes over open seafloor to the north of Line I, for which a density reference column within the mapped seafloor was established.

A similar procedure was followed for the region between the Dean Island Ridge and the Wright Island Ridge with Line F serving as the master line. Line G does not extend seaward of Carney Island. It also does not cross Line F and thus cannot be pinned to it. As mentioned in the previous section, an inversion of Line G with a density reference column on Carney Island gave nearly identical results to an inversion pinned to its intersection with Line 04, which is in turn pinned to Line F. The mean difference between the two inversions in regions of floating ice is 23.0 ± 24.2 m. We use the inversion pinned to Line 04 to maintain an internally consistent set of inversions. Line 2C crosses only Line 21. We pinned it by establishing its density reference profile at its crossing with Line 21 with the depth held at the depth at that location on Line 21. This portion of Line 21, between Wright Island and Dean Island is pinned to Line F.

We find that if longer sections of the E-W lines that extend from the Martin Peninsula past Line F are inverted, inversions pinned to Line I are consistently deeper than those pinned to Line F by 100–150 m. This observation suggests a change in crustal structure along the length of the GIS such that crustal density beneath Line I is greater or the crust is thinner (or both) than beneath Line F. This is consistent with an unpublished inversion of gravity data over grounded ice in the eastern ASE for density variations by one of the authors (K. J. T.), which showed higher densities under the Martin Peninsula than in areas farther east or south. It appears that the region of higher crustal density extends westward past our Line I.

We do not have any lines extending seaward of the ice shelf to mapped seafloor between Carney Island and Wright Island, so it is not immediately clear where the crustal boundary is located. We assume the boundary is within the ridge extending through Wright Island and the Scott Peninsula. The reason for this choice is that inversions of E-W lines pinned to Line F give lower residual gravity anomalies over grounded ice on Carney and Duncan islands than do lines pinned to Line I, while the average residual anomalies over grounded ice on Wright Island and the Scott Peninsula are comparable.

In the western GIS, to the west of the Dean Island Ridge, Lines D and C extend seaward of the ice shelf to areas with mapped seafloor. We find that east-west lines pinned to Line D are consistently about 100 m deeper than those pinned to Line C. If we utilize longer sections of the east-west lines that also cross Line F, we find that inversions pinned to Line D and to Line F are in general agreement, but deeper than inversions of the same gravity line pinned to Line C. This suggests a change in the geologic structure of the bedrock underlying the GIS at a location between Line D and Line C. The sense of the mismatch is that denser bedrock and/or a thinner crust is found under Lines D and F than under Line C.

LeMasurier and Rex (1989) state that the variety of volcanic rocks on Grant and Shepard islands and, in particular, the presence of felsic volcanics on Shepard Island suggest that the volcanics on the two islands represent the early stages of the construction of a shield volcano and that the islands may form the northern end of a band of volcanic activity extending north from the Ames Range (Figure 1). This suggests that a band extending south from Grant and Shepard islands may be affected by volcanic intrusions into the crust that could alter the average crustal density and/or thickness. We address this by leaving a gap of 5–10 km at about 129°30′W on E-W profiles between seafloor depths to the west determined from "pinning" the line to Line C and to the east "pinned" to Line D. We have chosen the boundary to be located at a gravity gradient that could result from the change in crustal structure. However, since we do not know the exact location or width of the change in crustal structure, the depths near the transition have an increased uncertainty. We also do not know how far the area of magmatically affected crust extends to the west of Shepard Island. Thus, the uncertainty increases in our inversions of the westernmost portions of Lines 21 and 03.

Our final inversions for the western portion of the E-W lines are shown in Figure 6, and the inversions for the central and eastern portions of the GIS are shown in Figures 7 and 8, respectively. We did not include an inversion of Line 05 to the west of the Scott Peninsula in the final results. This portion of the line crosses the north-south lines in the area where we infer sediment-filled overdeepenings so those lines do not provide accurate depths to serve to tie Line 05. In addition, due to a gap in the gravity data, the westernmost portion

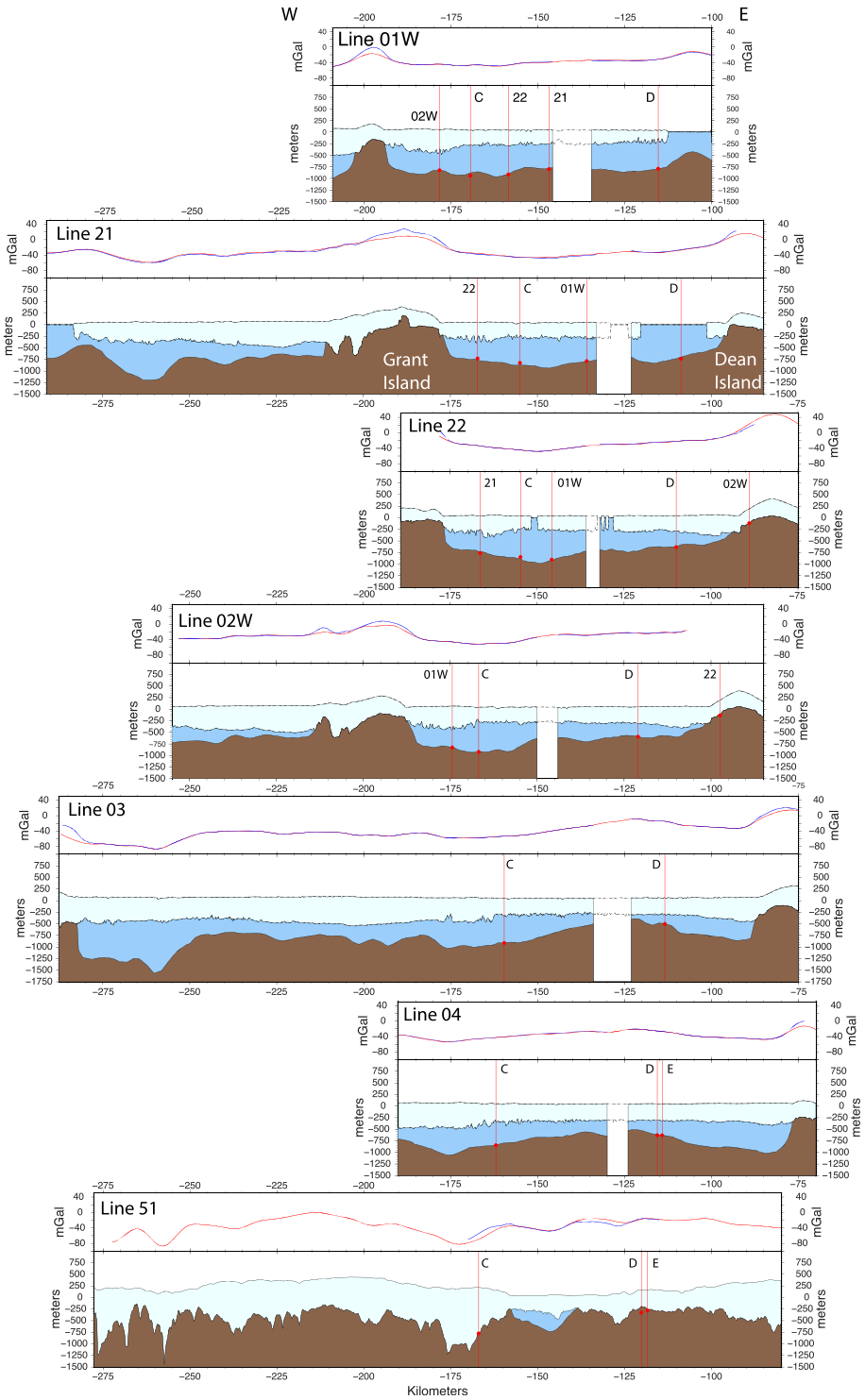

Figure 6. Geophysical profiles for the portions of the east-west lines across the western Getz Ice Shelf. The eastern end of each profile is over grounded ice on Dean Island or the island's submerged extension seaward of the ice shelf. For each profile, the upper panel shows the observed free-air gravity in red and the anomaly predicted by the inversion in blue. Lower panels show OIB geophysical profiles. Upper and lower surfaces of the ice are from lidar and radar, respectively. Where ice is grounded, the bed is determined from radar measurements. Where ice is floating, bathymetry is from inversion of gravity anomalies. Vertical red lines show intersections with north-south lines. Bathymetry/bed depth on the cross lines is shown as red dots. Line 01W is projected along N65.5°E. Other lines are projected along N87°E. The distance origin for each profile is at 125°W.

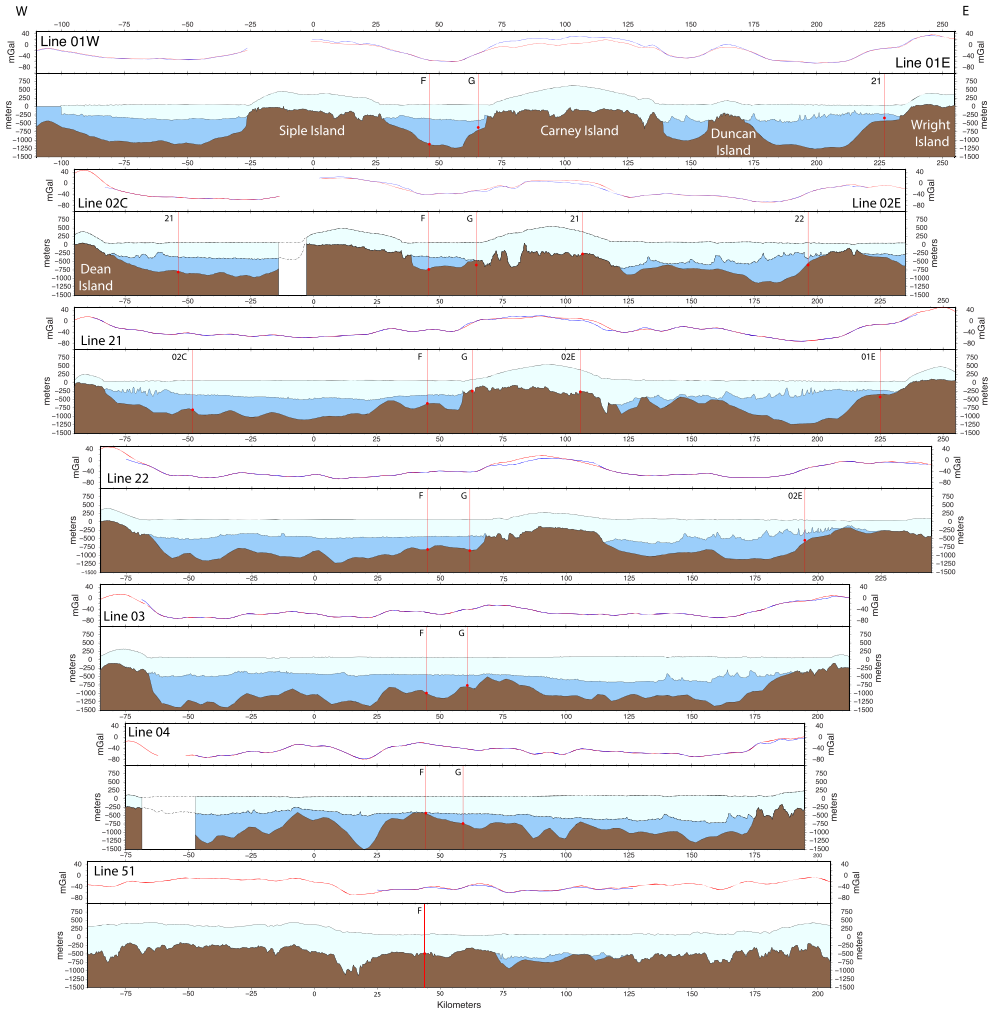

Figure 7. As in Figure 6, but showing the portions of the east-west lines across the central Get Ice Shelf. The western end of each profile is over grounded ice on Dean Island or at the island's submerged extension seaward of the ice shelf. The eastern end of each profile is over grounded ice on Wright Island or the Scott Peninsula. Lines 01W and 2C are projected along N65.5°E. Lines 01E and 02E are projected along N97°E. Other lines are projected along N87°E. The distance origin for each profile is at 125°W.

of Line 04, labeled "4a" in Figure 1, does not cross another line and thus could not be tied into the other lines, and so we did not include an inversion of it in our final results.

3. Bathymetry Beneath the GIS

A map of bathymetry beneath the GIS and bed beneath adjacent ice sheet, gridded with 2-km node spacing and contoured at 100-m intervals, is shown in Figure 9. Data locations along flight lines are shown in white.

Figure 10 shows a map of the difference between the OIB airborne gravity determined bathymetry and the Bedmap2 bathymetry. These differences range from about +200 m (OIB bathymetry shallower) to −800 m (OIB bathymetry deeper). Due to the featureless nature of the Bedmap2 bathymetry (Figure 2), relief on the difference map (Figure 10) closely mimics relief in the OIB map (Figure 9). One indication of the improved resolution provided by our inversion is that, as will be discussed in detail below, the prominent troughs observed in the shipboard data seaward of the ice shelf can now be traced across the ice shelf to merge into troughs observed by radar under the ice sheet,

Two observations can immediately be drawn from Figure 9.

1. The GIS is underlain by three separate cavities.

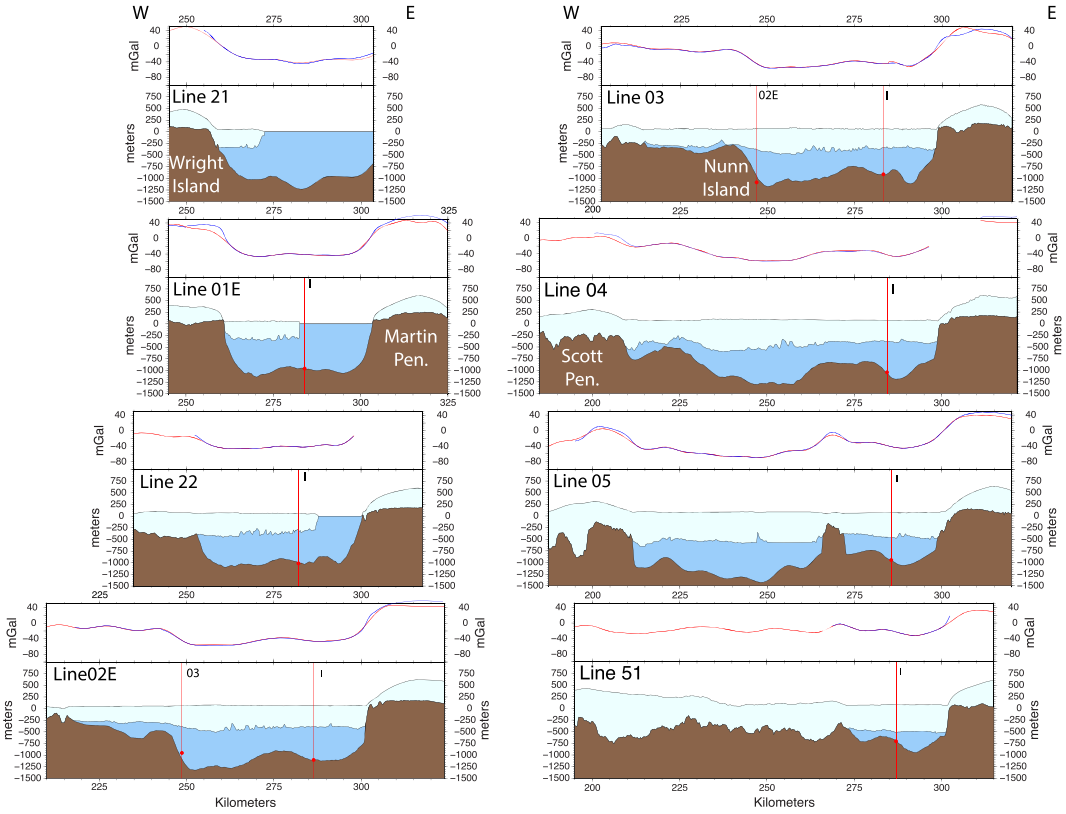

Figure 8. As in Figure 6, but showing the portions of the east-west lines across the eastern Getz Ice Shelf. Each profile except Line 21 extends from Wright Island/Scott Peninsula to the Martin Peninsula. Line 21 has its eastern end over open water north of the Martin Peninsula. Lines 01E and 02E are projected along N97°E. Other lines are projected along N87°E. The distance origin for each profile is at 125°W.

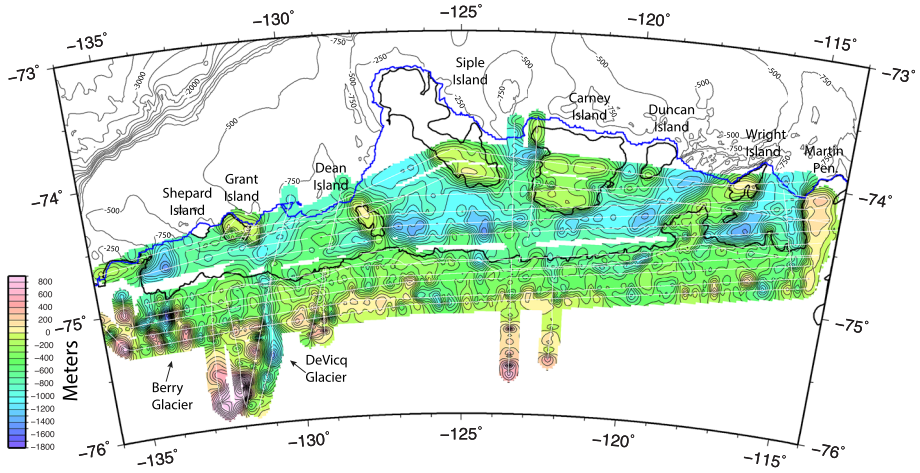

Figure 9. Bathymetry beneath the Getz Ice Shelf and bed beneath the adjacent ice sheet from Operation IceBridge data gridded with 2-km node spacing and contoured at 100-m intervals. Areas >10 km from a data point are masked. Color scale for the bathymetry/bed is shown in the inset on the lower left. Bathymetry under floating ice is from inversion of OIB gravity data, and bed under grounded ice is from OIB radar data. Data locations are in white. Heavy black lines show the Depoorter et al. (2013a) grounding line along the ice sheet and the 75-m elevation contour on the islands. Heavy blue line shows the approximate seaward edge of the ice shelf. IBCSO marine bathymetry (Arndt et al., 2013), contoured at 250-m intervals is shown on the continental shelf to the north of the gravity-determined bathymetry.

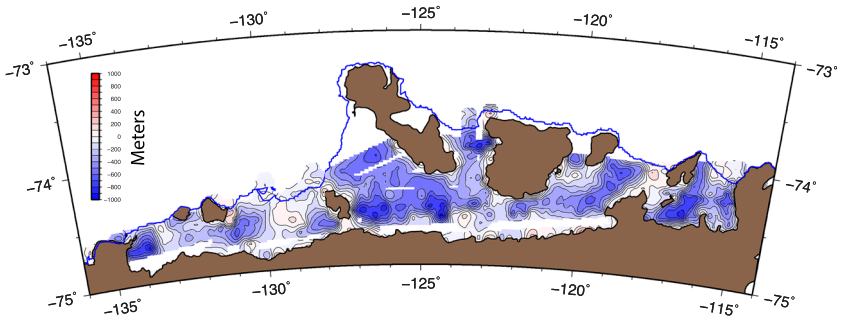

Figure 10. Map of the differences between our OIB gravity-derived bathymetry and Bedmap2 bathymetry gridded with 2-km node spacing and contoured at 100-m intervals. Areas >10 km from a gravity data point are masked. Color scale for the difference in bathymetry is shown in the inset on the upper left. Negative (blue-colored) regions indicate OIB bathymetry is deeper; positive (red-colored) regions indicate OIB bathymetry shallower. Heavy blue line shows the approximate seaward edge of the ice shelf.

All of the east-west OIB lines encounter grounded ice along two ridges extending from the ice front to the grounded ice sheet. One ridge extends along Dean Island to the ice sheet between 128°W and 127°W. The second extends from Wright Island near 116°30′W to the Scott Peninsula near 118°30′W. These two ridges thus appear to divide the GIS into three separate, effectively disjointed, cavities. However, since the OIB east-west lines over the ice shelf are spaced at distances of up to 11.3 km (at 127°30′W) over the Dean Island Ridge and 15.2 km (at 117°30′W) over the Wright Island Ridge, there is a question whether there are gaps in the grounded ridge and, if so, what the sill depth is in those gaps.

Figure 11a shows a map of the Reference Elevation Model of Antarctica (REMA) (Howat et al., 2019) ice surface elevation contoured at 10-m intervals, for the area of the Dean Island Ridge. The map shows that OIB Lines 04 and 05 are strategically placed just up onto the elevated surface of Dean Island and just landward of the ice sheet grounding line, respectively. Between these two lines, there is a region ~8 km wide with surface elevations mainly between 40 and 50 m. Such surface elevations in the GIS are associated with floating ice. Thus, there apparently is a passage between the western cavity and the central cavity to the south of Dean Island.

An important constraint on the significance of this passage for possible water flow between the western and central cavities of the GIS is the sill depth within the channel between Dean Island and the grounded ice sheet. The minimum bed depth measured by radar on Line 04 across the grounded southern end of Dean Island just to the north of the channel is 233 mbsl, while bed depth just south of the ice sheet grounding line on Line 05 is 255 mbsl. We have no direct measurement of the sea floor depth beneath the channel between Dean Island and the mainland between these two radar measurements.

The bed on Line 22, near the center of Dean Island (Figure 11a), reaches a radar-determined elevation of 41 meters above sea level (masl), while the radar-determined bed has a minimum depth of 99 mbsl on Line 04, near the southern end of Dean Island (Figures 6 and 7). Interpreted in the most simplistic manner, these observations imply a gradient in minimum bed depth along Dean Island of 12–15 m/km. Extrapolation of this gradient southward suggests that the bed could reach 350–400 mbsl beneath the floating ice south of Dean Island.

The southward bed gradient may also steepen to the south of Dean Island creating a deeper channel, but there is some evidence that this does not happen. Figure 11b shows the REMA surface elevation data in the region south of Dean Island outlined in white on Figure 11a, contoured at 5-m intervals. Figure 11c shows an ice surface profile along the line in blue on the lower panel. The profile crosses a 2.5-km-wide, 15-m-high ice rise located ~3 km south of Dean Island and marked by a red arrow. The ice rise indicates grounded ice, and so implies a high in the bed at that location. We cannot dismiss the possibility of a deep cleft in the bed in the 5 km between the ice rise and the grounded ice sheet. However, it appears more likely that the ice rise reflects a decrease in the bed gradient as it begins to level out before rising up toward the grounded ice sheet. In that case, shallow surface water could circulate between the Western and Central cavities, but deeper water will be confined within each cavity.

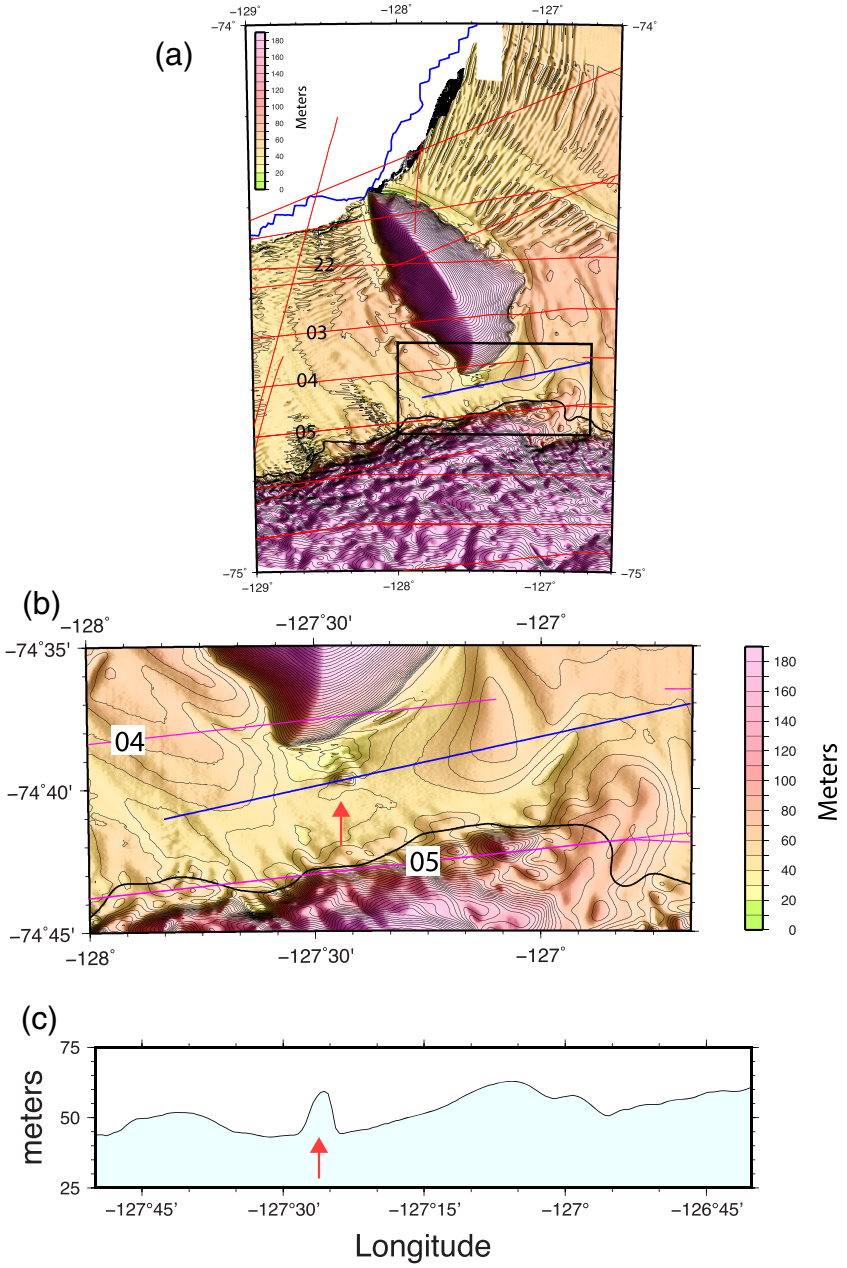

Figure 11. (a) shows the ice surface elevation in the vicinity of Dean Island from the Reference Elevation Model of Antarctica (REMA) (Howat et al., 2019) gridded at 100-m node spacing at contoured at 10-m intervals. Image is illuminated from the east, and color scale is shown as an inset. Heavy blue line shows the approximate edge of the ice shelf, and the heavy black line shows the Depoorter et al. (2013a) grounding line. OIB gravity lines are shown in red, and lines discussed in the text are labeled. White box shows the area of the map in (b) and the blue line within it gives the location of the elevation profile in (c). (b) shows surface elevation of the area between Dean Island and the West Antarctic Ice Sheet outlined by the white box in (a) from REMA gridded at 100-m node spacing and contoured at 5-m intervals. Image is illuminated from the east and color scale is shown to the right. Heavy black line shows the Depoorter et al. (2013a) grounding line. OIB gravity lines are shown in purple and lines discussed in the text are labeled. The blue line shows the location of the bathymetry profile shown in (c), and the red arrow shows the location of the ice rise discussed in the text. Horizontal axis of the profile in (c) is longitude to allow comparison to the map. At 74°40′S, 1° of longitude is ~29.4 km.

Figure 12a shows the REMA ice surface elevation contoured at 10-m intervals, in the region of the Scott Peninsula, Nunn Island, and Wright Island, which form the ridge separating the Central and Eastern cavities. The three topographic highs are separated by areas of relatively flat ice at an elevation of

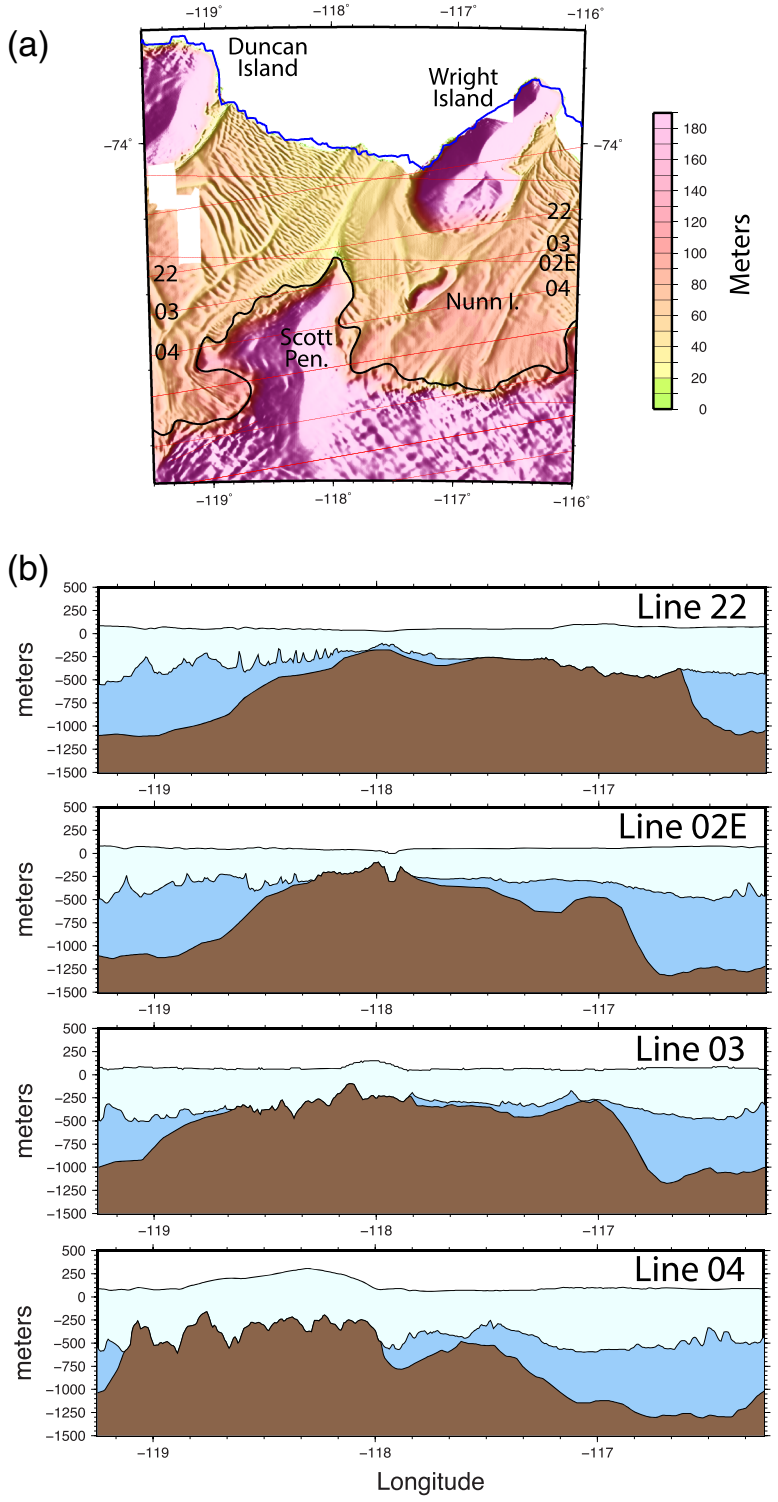

Figure 12. (a) Ice surface elevation in the vicinity of the Scott Peninsula and Wright Island from the Reference Elevation Model of Antarctica (REMA) (Howat et al., 2019) gridded at 100-m node spacing at contoured at 10-m intervals. Image is illuminated from the east and color scale is shown to the right. Heavy blue line shows the edge of the ice shelf, and the heavy black line shows the Depoorter et al. (2013a) grounding line. OIB gravity lines are shown in red, and lines discussed in the text are labeled. (b) OIB geophysical profiles across the Wright Island Ridge. Where ice is grounded, the bed is determined from radar measurements. Where ice is floating, bathymetry is from inversion of gravity anomalies. Location of lines is shown in (a). Horizontal axis of the profiles is longitude to allow comparison to the map. At these latitudes, 1° of longitude varies from ~30.1 km for Line 22 to ~29.8 km for Line 04.

40–60 mbsl, implying the presence of floating ice. Figure 12b shows four bathymetric profiles across the Wright Island Ridge. These confirm that grounded ice is not continuous over the entire ridge, but that areas of floating ice are found between Scott Peninsula and Nunn Island, and to the south of Wright Island. Line 22, which crosses the southern end of Wright Island and then passes just north of Scott Peninsula, is the critical profile in determining the sill depth between the Central Cavity and the Eastern Cavity. This line shows a maximum depth of 345 mbsl between Wright Island and Scott Peninsula. Thus, as with the Dean Island Ridge, there can be some transport of shallow water between the cavities, but the deeper water is confined to a single cavity.

2. Deep troughs extend from the ice front to valleys in the ice sheet bed in all three cavities.

The gravity inversion reveals that deep troughs (>900 mbsl) are present in all three cavities. The troughs extend from seaward of the ice shelf beneath the ice shelf, connecting to valleys in the bed beneath the ice sheet. Extending under the ice for 50 to >100 km, these troughs provide potential pathways for warm mCDW to access the inner portions of the ice shelf and the grounding line.

In the Western Cavity, there are two troughs. The westernmost extends from the ice front just east of 134°W toward a trio of glaciers (Berry, Venzke, and Johnson) that drain into the southwestern corner of the GIS. This trough reaches a depth of >1,500 mbsl near 133°50′W on Line 03 (260 km on Figure 6). The bathymetric contours in Figure 9 show rapid shallowing landward of Line 03, but this appears to be a gridding artifact resulting from the relatively large data gap between Lines 03 and 06. There is probably a broad area of deep seafloor under the ice shelf west of about 133°30′W. Berry Glacier is the largest of the glaciers feeding into this area. It is underlain by a 10- to 15-km-wide, steep-sided trough, which reaches a radar-determined depth of 1,949 mbsl on Line 07 near 75°S, 19 km landward of the grounding line. This narrow glacial trough shallows southward but is still at a radar-determined depth of 1,102 mbsl on OIB Line 10, 45.5 km south of the grounding line.

The second trough in the Western Cavity extends southwest from the ice front at 130°W to just off the southeast corner of Grant Island, where it turns south and continues into a trough beneath DeVicq Glacier. This trough has a fairly consistent depth in the range of ~950 mbsl to ~1,050 mbsl across the width of the ice shelf. The apparent shallowing of the trough in the vicinity of the grounding line in Figure 9 again appears to be a gridding artifact due to the relatively large spacing between east-west lines crossing the trough. The narrow, deep trough under DeVicq Glacier continues inland to at least 75°30′S. Maximum depths recorded on OIB radar lines across it vary from 820 to 1,550 mbsl.

Within the Central Cavity, troughs extend landward from the ice front between Dean and Siple islands and between Duncan and Wright islands, but no through-going troughs are observed within the cavity openings on either side of Carney Island.

The trough between Siple and Dean islands extends southwest along the western edge of Siple Island to ~74° 20′S where it bifurcates. One branch continues southward toward a subglacial valley under the ice sheet just to the east of 125°W. The other extends to the west, where it appears to terminate close to the eastern end of Dean Island, although it may continue south along the eastern edge of the Dean Island Ridge into a shallow valley under the ice sheet.

The eastern portion of the Central Cavity is characterized by a trough between Duncan and Wright islands that extends southwest along the western edge of the Wright Island Ridge to about 74°25′S with depths of 1,100–1,300 mbsl. It then turns west and runs along the southern edge of Carney Island to about 122°W where it turns south into a valley beneath the ice sheet. There is probably a second branch of this trough, masked by gridding artifacts due to spacing of east-west lines, that continues south to a subglacial valley beneath the ice sheet near 120°W.

No through-going trough is present between Siple and Carney islands. Marine bathymetric data show a trough approaching 1,000 mbsl seaward of the ice shelf between Siple and Carney islands. This area of deep water extends between the islands as far as Line 01E and the seaward portions of Lines F and G (Figures 5, 7, and 9). However, the seafloor between the two islands appears to shallow rapidly southward, and Lines 02E, F, and 21 give seafloor depths of 600–800 mbsl to the south of 74°S. Similarly, Line 01E gives a maximum depth of about 1,000 mbsl between Carney and Duncan islands, but Lines 02E and 21 show that the seafloor shallows rapidly southward to 500–700 mbsl (Figures 7 and 9).

The Eastern Cavity is characterized by a bathymetric trough also observed on marine data seaward of the ice shelf opening between Wright Island and the Martin Peninsula. Beneath the ice shelf, it divides into two separate troughs. The deeper of the two, with depths of 1,000–1,300 mbsl, extends SW along the eastern edge of the Wright Island Ridge. The second trough extends along the western edge of the Martin Peninsula with depths ranging from 900 to 1,100 mbsl. Both troughs connect with subglacial valleys beneath the ice sheet.

4. Summary and Conclusions

We present, document, and discuss a geologically consistent inversion of NASA OIB airborne gravity data for bathymetry beneath the GIS, which extends for ~650 km along the Amundsen Sea coast of Antarctica. Our new bathymetry is a significant advance from the Bedmap2 bathymetry, which is derived from a spline interpolation between ice-penetrating radar data in grounded areas and shipboard bathymetry measurements seaward of the ice shelf with no in situ data from the ice shelf.

The GIS consists of three separate cavities. Two topographic ridges extend completely across the ice shelf. The Wright Island Ridge extends from the ice front near 116°30′W through Wright Island to the Scott Peninsula near 118°30′W. The Dean Island Ridge extends through Dean Island from the ice front to the mainland between 127°W and 128°W. Ice is grounded along most of these ridges but limited areas of floating ice between Wright Island and Scott Peninsula between Dean Island and the mainland permit possible movement of shallow water between the cavities. The sill depth in both gaps is ~ 400 mbsl.

Bathymetric troughs at depths consistently >900 mbsl extend beneath the ice shelf from the ice front to subglacial valleys under the ice sheet in all three cavities, providing potential pathways for relatively warm mCDW to access the inner portions of the ice shelf and the grounding line. Our inversions of OIB airborne gravity data also allow us to infer the presence of thick (400–1,300 m) accumulations of sediment within overdeepenings near the grounding line.

Data Availability Statement

The NASA Operation IceBridge airborne data and the inversions for bathymetry used in this paper are archived by the National Snow and Ice Data Center and are available at http://nsidc.org/data/icebridge.

Acknowledgments

We thank the aircrews and instrument teams on the OIB deployments during which these data were collected and, in particular, the LDEO and SGL gravity crews. We thank Jonny Kingslake and Stan Jacobs for valuable comments and suggestions that greatly improved the manuscript and David Porter for helpful discussions. We also thank Michael Wood and two anonymous reviewers for useful comments. The GMT software package (Wessel & Smith, 1998) was used extensively in data analysis and preparation of figures. This work was supported by NASA grants NNX09AR49G, NNX10AT69G, NNX13AD25A, and NNX16J65G.

References

Allen, C., Leuschen, C., Gogineni, P., Rodriguez-Morales, F., & Paden, J. (2010). IceBridge MCoRDS L2 Ice Thickness, NASA National Snow and Ice Data Center Distributed Active Archive Center, Boulder CO. https://doi.org/10.5067/GDQ0CUCVTE2Q

Argyle, M., Ferguson, S., Sander, L., & Sander, S. (2000). AIRGrav results: A comparison of airborne gravity data with GSC test site data. *The Leading Edge*, *19*, 1134–1138.

Arndt, J. S., Schenke, H. W., Jakobsson, M., Nitsche, F. O., Buys, G., Goleby, B., et al. (2013). The International Bathymetric Chart of the Southern Ocean (IBCSO) Version 1.0—A new bathymetric compilation covering circum-Antarctic waters. *Geophysical Research Letters*, *40*, 3111–3117. https://doi.org/10.1002/grl.50413

Assmann, K. M., Darelius, E., Wahlin, A. K., Kim, T. W., & Lee, S. H. (2019). Warm circumpolar deep water at rhe western Getz Ice Shelf, Antarctica. *Geophysical Research Letters*, *46*, 870–878. https://doi.org/10.1029/2018GL081354

Boghosian, A., Tinto, K. J., Cochran, J. R., Porter, D., Elieff, S., Burton, B. L., & Bell, R. E. (2015). Resolving fjord bathymetry from airborne gravity along Greenland fjords. *Journal of Geophysical Research: Solid Earth*, *120*, 8516–8533. https://doi.org/10.1002/2015JB012129

Cochran, J. R., & Bell, R. E. (2012). Inversion of IceBridge gravity data for continental shelf bathymetry beneath the Larsen Ice Shelf, Antarctica. *Journal of Glaciology*, *58*, 540–552. https://doi.org/10.3189/2012JoG11J033

Cochran, J. R., Jacobs, S. S., Tinto, K. J., & Bell, R. E. (2014). Bathymetric and oceanic controls on Abbot Ice Shelf thickness and stability. *The Cryosphere*, *8*, 877–889. https://doi.org/10.5194/tc-8-877-2014

Depoorter, M. A., Bamber, J. L., Griggs, J. A., Lenaerts, J., Ligtenberg, S. R. M., van den Broeke, M. R., & Moholdt, G. (2013a). Antarctic grounding line, *PANGAEA,* https://doi.org/10.1594/PANGAEA.819150

Depoorter, M. A., Bamber, J. L., Griggs, J. A., Lenaerts, J., Ligtenberg, S. R. M., van den Broeke, M. R., & Moholdt, G. (2013b). Calving fluxes and basal melt rates of Antarctic ice shelves. *Nature*, *502*, 89–93. https://doi.org/10.1038/nature12567

Dupont, T. K., & Alley, R. B. (2005). Assessment of the importance of ice-shelf buttressing to ice-shelf flow. *Geophysical Research Letters*, *32*, L04503. https://doi.org/10.1029/2004GL022024

Förste, C., Schmidt, R., Stubenvoll, R., Flechtner, F., Meyer, U., Konig, R., et al. (2008). The GeoForschungsZentrum Potsdam/Groupe de Recherche de Geodesie Spatiale satellite-only and combined gravity field models: Eigen-GL04S1 and Eigen-GL04C. *Journal of Geodesy*, *82*, 331–346. https://doi.org/10.1007/s00190-007-0183-8

Fretwell, P., Pritchard, H. D., Vaughan, D. G., Bamber, J. L., Barrand, N. E., Bell, R. E., et al. (2013). Bedmap2: Improved ice bed, surface and thickness datasets for Antarctica. *The Cryosphere*, *7*, 375–393. https://doi.org/10.5194/tc-7-375-2013

Gogineni, P., Yan, J. B., Paden, J., Leuschen, C., Li, J., Rodriguez-Morales, F., et al. (2014). Bed topography of Jakobshaven Isbrae, Greenland, and Byrd Glacier, Antarctica. *Journal of Glaciology*, *60*(223), 813–833. https://doi.org/10.3189/2014JoG14J129

Graham, A. G. C., Larter, R. D., Gohl, K., Hillenbrand, C. D., Smith, J. A., & Kuhn, G. (2009). Bedform signature of a West Antarctic palaeo-ice stream reveals a multi-temporal record of flow and substrate control. *Quaternary Science Reviews*, *28*, 2774–2793. https://doi.org/10.1016/j.quascirev.2009.07.003

Gudmundsson, G. H. (2013). Ice-shelf buttressing and the stability of marine ice sheets. *The Cryosphere*, *7*, 647–655. https://doi.org/10.5194/tc-7-647-2013

Howat, I. M., Porter, C., Smith, B. E., Noh, M. J., & Morin, P. (2019). The Reference Elevation Model of Antarctica. *The Cryosphere*, *13*, 665–674. https://doi.org/10.5194/tc-13-665-2019

Jacobs, S. S., Giulivi, C. F., Dutrieux, P., Rignot, E., Nitsche, F. O., & Mouginot, J. (2013). Getz Ice Shelf melting response to changes in ocean forcing. *Journal of Geophysical Research: Oceans*, *118*, 1–17. https://doi.org/10.1002/jgrc20298

Jacobs, S. S., Hellmer, H. H., Doake, C. S. M., Jenkins, A., & Frolich, R. M. (1992). Melting of ice shelves and mass balance of Antarctica. *Journal of Glaciology*, *38*, 375–387.

Jacobs, S. S., Hellmer, H. H., & Jenkins, A. (1996). Antarctic ice sheet melting in the southeast Pacific. *Geophysical Research Letters*, *23*, 957–960.

Jacobs, S. S., Jenkins, A., Giulivi, C. F., & Dutrieux, P. (2011). Stronger ocean circulation and increased melting under Pine Island Glacier ice shelf. *Nature Geoscience*, *4*, 519–523. https://doi.org/10.1038/NGEO1188

Jacobs, S. S., Jenkins, A., Hellmer, H. H., Giulivi, C. F., Nitsche, F. O., Huber, B. A., & Guerrero, R. (2012). The Amundsen Sea and the Antarctic Ice Sheet. *Oceanography*, *25*, 154–163. https://doi.org/10.5670/oceanog.2012.90

Jenkins, A., Dutrieux, P., Jacobs, S. S., McPhail, S. D., Perrett, J. R., Webb, A. T., & White, D. (2010). Observations beneath Pine Island Glacier in West Antarctica and implications for its retreat. *Nature Geoscience*, *3*, 468–472. https://doi.org/10.1038/NGEO890

Krabill, W. (2014). IceBridge ATM L2 Icessn Elevation, Slope, and Roughness, Version 2. NASA National Snow and Ice Data Center Distributed Active Archive Center, Boulder CO. https://doi.org/10.5067/FCCzIIFRPZ30

Krabill, W., Abdalati, W., Frederick, E. R., Manizade, S. S., Martin, C. F., Sonntag, J. G., et al. (2002). Aircraft laser altimetry measurement of elevation changes of the Greenland Ice Sheet: Techniques and accuracy assessment. *Journal of Geodynamics*, *34*(3–4), 357–376.

Larter, R. D., Graham, A. G. C., Gohl, K., Kuhn, G., Hillenbrand, C. D., Smith, J. A., et al. (2009). Subglacial bedforms reveal complex basal regime in a zone of paleo-ice stream convergence, Amundsen Sea embayment, West Antarctica. *Geology*, *37*, 411–414. https://doi.org/10.1130/G25505A.1

le Brocq, A., Payne, A. J., & Vieli, A. (2010). An improved Antarctic dataset for high resolution numerical ice sheet models (ALBMAP v1). *Earth System Science Data*, *2*, 247–260. https://doi.org/10.5194/essd-2-247-2010

LeMasurier, W. E. (1990). Marie Byrd Land. In W. E. LeMasurier, J. W. Thomson, P. E. Baker, P. R. Kyle, P. D. Rowley, J. L. Smellie, & W. J. Verwoerd (Eds.), *Volcanoes of the Antartic Plate and Southern Ocean*, *Antarctic Research Series* (Vol. 48, pp. 147–255). Washington: American Geophysical Union.

LeMasurier, W. E., & Rex, D. C. (1989). Evoluyion of linear volcanic ranges in Marie Byrd Land, West Antarctica. *Journal of Geophysical Research*, *94*, 7223–7236.

Leuschen, C. (2011). IceBridge MCoRDS L1B Geolocated Radar Echo Strength Profiles, V01.3, digital media, National Snow and Ice Data Center, Boulder, Colorado.

Liu, Y., Moore, J. C., Cheng, X., Gladstone, R. M., Bassis, J. N., Liu, H., et al. (2015). Ocean-driven thinning enhances iceberg calving and retreat of Antarctic ice shelves. *Proceedings of the National Academy of Sciences of the United States of America*, *112*, 3263–3268. https://doi.org/10.1073/pnas.1415137112

Lowe, A. L., & Anderson, J. B. (2002). Reconstruction of the West Antarctic ice sheet in Pine Island Bay during the Last Glacial Maximum and its subsequent retreat history. *Quaternary Science Reviews*, *21*, 1879–1897.

Lowe, A. L., & Anderson, J. B. (2003). Evidence for abundant subglacial meltwater beneath the paleo-ice sheet in Pine Island Bay, Antarctica. *Journal of Glaciology*, *49*, 125–138.

Martin, C. F., Krabill, W. B., Manizade, W. B., Russel, R. L., Sonntag, J. G., Swift, R. N., & Yungel, J. K. (2012). Airborne Topographic Mapper calibration procedures and accuracy assessment, 32 pp., NASA Technical Report NASA/TM-2012-215891, Greenbelt, MD.

McMillan, M., Shepherd, A., Nienow, P., & Leeson, A. (2011). Tide model accuracy in the Amundsen Sea, Antarctica, from radar interferometry observations of ice shelf motion. *Journal of Geophysical Research*, *116*, C11008. https://doi.org/10.1029/2011JC007294

Millan, R., St. Laurent, P., Rignot, E., Morlighem, M., Mougenot, D., & Scheuchl, B. (2020). Constraining an ocean model under Getz Ice Shelf, Antarctica, using a gravity-derived bathymetry. *Geophysical Research Letters*, *47*, e2019GL086522. https://doi.org/10.1029/2019GL086522

Morlighem, M., Rignot, E., Binder, T., Blankenship, D. D., Drews, R., Eagles, G., et al. (2020). Deep glacial troughs and stabilizing ridges unveiled beneath the margins of the Antarctic Ice Sheet. *Nature Geoscience*, *13*, 132–137. https://doi.org/10.1038/s41561-019-0510-8

Muto, A., Anandakrishnan, S., & Alley, R. B. (2013). Subglacial bathymetry and sediment layer distribution beneath the Pine Island Glacier ice shelf, West Antarctica, modeled using aerogravity and autonomous underwater vehicle data. *Annals of Glaciology*, *54*, 27–32. https://doi.org/10.3189/2013AoG64A110

Muto, A., Peters, L. E., Gohl, K., Sasgen, I., Alley, R. B., Anandakrishnan, S., & Riverman, K. L. (2016). Subglacial bathymetry and sediment distribution beneath Pine Island Glacier Ice Shelf modeled using aerogravity and in situ geophysical results: New results. *Earth and Planetary Science Letters*, *433*, 63–75. https://doi.org/10.1016/j.epsl.2015.10.037

Nitsche, F. O., Gohl, K., Larter, R. D., Hillenbrand, C. D., Kuhn, G., Smith, J. A., et al. (2013). Paleo ice flow and subglacial meltwater dynamics in Pine Island Bay, West Antarctica. *The Cryosphere*, *7*, 249–262. https://doi.org/10.5194/tc-7-249-2013

Nitsche, F. O., Jacobs, S. S., Larter, R. D., & Gohl, K. (2007). Bathymetry of the Amundsen Sea continental shelf: Implications for geology, oceanography and glaciology. *Geochemistry, Geophysics, Geosystems*, *8*, Q10009. https://doi.org/10.1029/12007GC001694

Padman, L., Fricker, H. A., Coleman, R., Howard, S., & Erofeeva, L. (2002). A new tidal model for the Antarctic ice shelves and seas. *Annals of Glaciology*, *34*, 247–254.

Paolo, F. S., Fricker, H. A., & Padman, L. (2015). Volume loss from Antarctic ice sheets is accelerating. *Science*, *348*(6232), 327–331. https://doi.org/10.1126/science.aaa0940

Pritchard, H. D., Ligtenberg, S. R. M., Fricker, H. A., Vaughan, D. G., van der Broeke, M. R., & Padman, L. (2012). Antarctic ice-sheet loss driven by basal melting of ice shelves. *Nature*, *484*, 502–505. https://doi.org/10.1038/nature10968

Rignot, E. (2008). Changes in West Antarctic ice stream dynamics observed with ALOS PALSAR data. *Geophysical Research Letters*, *35*, L12505. https://doi.org/10.1029/2008GL033365

Rignot, E., Jacobs, S. S., Mouginot, J., & Scheuchl, B. (2013). Ice shelf melting around Antarctica. *Science*, *341*, 266–270. https://doi.org/10.1126/science1235798

Sander, S., Argyle, M., Elieff, S., Ferguson, S., Lavoie, V., & Sander, L. (2004). The AIRGrav aiborne gravity system. In R. Lane (Ed.), *Airborne Gravity 2004—Australian Society of Exploration Geophysicists Workshop* (pp. 49–53). Canberra, Australia: Geoscience Australia. http://sgl.com/technicalpapers/AIRGrav_airborne_grav_sys.pdf

Seroussi, H., Nakayama, Y., Larour, E., Menemenlis, D., Morlighem, M., Rignot, E., & Khazendar, A. (2017). Continued retreat of Thwaites Glacier, West Antarctica, controlled by bed topography and ocean circulation. *Geophysical Research Letters*, *44*, 6191–6199. https://doi.org/10.1002/2017GL072910

Shepherd, A., Wingham, D., & Rignot, E. (2004). Warm ocean is eroding West Antarctica. *Geophysical Research Letters*, *31*, L23402. https://doi.org/10.1029/2004GL021106

Studinger, M., Bell, R. E., & Frearson, N. (2008). Comparison of AIRGrav and GT-1A airborne gravimeters for research applications. *Geophysics*, *73*, 151–161. https://doi.org/10.1190/1.2969664

Talwani, M., Worzel, J. L., & Landisman, M. (1959). Rapid gravity computations for two-dimensional bodies with application to the Mendocino submarine fracture zone. *Journal of Geophysical Research*, *64*, 49–59.

Thoma, M., Jenkins, A., Holland, D., & Jacobs, S. S. (2008). Modeling Circumpolar Deep Water intrusions on the Amundsen Sea continental Shelf, Antarctica. *Geophysical Research Letters*, *35*, L18602. https://doi.org/10.1029/2008GL034939

Timmermann, R., le Brocq, A., Deen, T. J., Domack, E. W., Dutrieux, P., Galton-Fenzi, B., et al. (2010). A consistent data set of Antarctic ice sheet topography, cavity geometry, and global bathymetry. *Earth System Science Data*, *2*, 261–273. https://doi.org/10.5194/essd-2-261-2010

Tinto, K. J., Bell, R. E., & Cochran, J. R. (2019). IceBridge Sander AIRGrav L1B Geolocated Free Air Gravity Anomalies,*NASA National Snow and Ice Data Center Distributed Active Archive Center, Boulder CO*. https://doi.org/10.5067/R1RQ6NRIJV89

Turner, J., Orr, A., Gudmundsson, G. H., Jenkins, A., Bingham, R. G., Hillenbrand, C. D., & Bracegirdle, T. J. (2017). Atmosphere-ocean-ice interactions in the Amundsen Sea Embayment, West Antarctica. *Reviews of Geophysics*, *55*, 235–276. https://doi.org/10.1002/2016RG000532

Wellner, J. S., Lowe, A. L., Shipp, S. S., & Anderson, J. B. (2001). Distribution of glacial geomorphic features on the Antarctic continental shelf and correlation with substrate: Implications for ice behavior. *Journal of Glaciology*, *47*, 397–411.

Wessel, P., & Smith, W. H. F. (1998). New improved version of Generic Mapping Tools released. *EOS Transactions of American Geophysical Union*, *79*, 579.